2008

Lyapunov-Schmidt reduction algorithm for three-dimensional discrete vortices

M Lukas

D Pelinovsky

PG Kevrekidis
University of Massachusetts - Amherst, kevrekid@math.umass.edu

Lyapunov–Schmidt reduction algorithm for three-dimensional discrete vortices

Mike Lukas[†], Dmitry Pelinovsky[†] and P.G. Kevrekidis[††]
[†] Department of Mathematics, McMaster University, Hamilton, Ontario, Canada, L8S 4K1
[††] Department of Mathematics and Statistics, University of Massachusetts, Amherst, MA 01003

February 4, 2008

Abstract

We address persistence and stability of three-dimensional vortex configurations in the discrete nonlinear Schrödinger (NLS) equation and develop a symbolic package based on Wolfram's MATHEMATICA for computations of the Lyapunov–Schmidt reduction method. The Lyapunov–Schmidt reduction method is a theoretical tool which enables us to study continuations and terminations of the discrete vortices for small coupling between lattice nodes as well as the spectral stability of the persistent configurations. The method was developed earlier in the context of the two-dimensional NLS lattice and applied to the on-site and off-site configurations (called the vortex cross and the vortex cell) by using semi-analytical computations [18, 19]. The present treatment develops a full symbolic computational package which takes a desired waveform at the anti-continuum limit of uncoupled sites, performs a required number of Lyapunov–Schmidt reductions and outputs the predictions on whether the configuration persists, for finite coupling, in the three-dimensional lattice and whether it is stable or unstable. It also provides approximations for the eigenvalues of the linearized stability problem. We report a number of applications of the algorithm to important multi-site configurations, such as the simple cube, the double cross, and the diamond. For each three-dimensional configuration, we identify exactly one solution, which is stable for small coupling between lattice nodes.

1 Introduction

Over the last decade, the topic of nonlinear dynamical lattices and of the coherent structures that arise in them has attracted considerable attention. This can be mainly attributed to a diverse set of research themes where the corresponding mathematical models have emerged as an appropriate description of the physical problem. Such areas include, but are not limited to, arrays of nonlinear-optical waveguides [1] and photorefractive crystal lattices [2], Bose-Einstein condensates (BECs) trapped in optical lattices (OLs) [3], Josephson-junction ladders [4], micro-mechanical models of cantilever arrays [5] or even simple models of the complex dynamics of the DNA double strand [6]. These, in turn, have spurted an increasing mathematical interest in Hamiltonian discrete systems and produced a considerable volume of theoretical results, which has partially been summarized in the reviews [7].

Arguably, the most prototypical among the discrete nonlinear Hamiltonian models is the discrete nonlinear Schrödinger equation (DNLS) [8], which results from a centered-difference discretization of

its famous continuum analog, the nonlinear Schrödinger equation (NLS) [9]. The DNLS arises most notably in the nonlinear optics of waveguide arrays, where it was developed [10] as an envelope wave description of the electric field in each of the waveguides. It was also systematically derived as a tight-binding model for Bose-Einstein condensates trapped in, so-called, optical lattices [11]. In other settings, such as e.g. photorefractive crystals, the validity of the DNLS model is more limited, yet still a lot of its qualitative features can be observed even experimentally. It is for this reason that this simple yet rich model has been used to justify numerous experimental observations in the above-mentioned areas, including the formation of discrete solitons [12], the existence of Peierls-Nabarro barriers for such waves [13], the modulational instability of uniform states both in optical [14] and in BEC [15] experiments, and the formation of discrete vortices [16] in two-dimensions, among many others. In the earlier work of [17] and [18, 19], we studied systematically the solutions that can be obtained in the one- and two-dimensional installments of the model respectively, using a combination of methods of Lyapunov-Schmidt reductions and perturbation theory in the, so-called, anti-continuum limit of lattice sites uncoupled with each other.

In the present paper, we provide a mathematical framework and a symbolic package for the systematic computations of the existence and the stability of localized states in the fully three-dimensional DNLS model. To the best of our knowledge, this is the first time that systematic stability results are developed for the three-dimensional system. Earlier numerical work in [20, 21] revealed a considerable wealth of possible states, including octupoles, diamonds and vortex cubes, among many others. It is these states and different variants thereof that our systematic methodology addresses in the present publication, by formulating a symbolic approach that can be straightforwardly used to study the potential persistence and linear stability of *any* desired configuration.

Our results on the three-dimensional DNLS model cannot be applied to dynamics of waveguide arrays since the third spatial direction in the optical problem represents the evolution time variable. However, the model is still relevant to BECs and an additional possibility for its physical realization is offered by a three-dimensional crystal built of microresonators [22].

Our article is structured as follows. Section 2 formulates the mathematical problem of interest. Section 3 presents the main results for the development of the computational algorithm based on the Lyapunov–Schmidt reduction method. Section 4 reports the application of the computational algorithm to three kinds of three-dimensional vortex configurations. Section 5 compares these results with direct numerical bifurcation results of the three-dimensional DNLS model. Section 6 concludes the paper. Appendix A contains typical outputs of the MATHEMATICA software package.

2 Formulation of the problem

We consider the discrete nonlinear Schrödinger (NLS) equation in three spatial dimensions:

$$i\dot{u}_n + \epsilon \Delta u_n + |u_n|^2 u_n = 0, \qquad n \in \mathbb{Z}^3, \;\; t \in \mathbb{R}_+, \;\; u_n \in \mathbb{C}, \tag{2.1}$$

where $\epsilon > 0$ is the coupling strength (which can also be thought of as the reciprocal squared lattice spacing) and Δu_n is the discrete three-dimensional Laplacian

$$\Delta u_n = u_{n+e_1} + u_{n-e_1} + u_{n+e_2} + u_{n-e_2} + u_{n+e_3} + u_{n-e_3} - 6u_n, \qquad n \in \mathbb{Z}^3,$$

with $\{e_1, e_2, e_3\}$ being standard unit vectors on $\mathbb{Z}^3$. The discrete NLS equation (2.1) is a Hamiltonian system with the Hamiltonian function

$$H = \epsilon \sum_{j=1}^{3} \|u_{n+e_j} - u_n\|^2_{l^2(\mathbb{Z}^3)} - \frac{1}{2}\|u_n\|^4_{l^4(\mathbb{Z}^3)}, \tag{2.2}$$

which is referred to as the energy of the discrete system. Due to invariance of the discrete NLS equation (2.1) with respect to time translation $u_n(t) \mapsto u_n(t - t_0)$, $\forall t_0 \in \mathbb{R}$, the energy H is constant in time, e.g. $H(t) = H(0)$. Another conserved quantity is the discrete l^2-norm, such that $Q = \|u_n(t)\|^2_{l^2(\mathbb{Z}^3)}$ and $Q(t) = Q(0)$, which is related to the invariance of the NLS equation (2.1) with respect to the gauge transformation $u_n(t) \mapsto u_n(t)e^{i\theta_0}$, $\forall \theta_0 \in \mathbb{R}$. The natural phase space of the discrete system is $X = l^2(\mathbb{Z}^3) \cap l^4(\mathbb{Z}^3)$.

Let $\mathbf{u}$ be an abstract vector for the triple-indexed doubly-infinite two-component sequences of real and imaginary parts of $\{u_n\}_{n\in\mathbb{Z}^3}$, such that the 2-block at the node $n \in \mathbb{Z}^3$ is

$$\mathbf{u}_n = \begin{bmatrix} \mathrm{Re}(u_n) \\ \mathrm{Im}(u_n) \end{bmatrix}.$$

Then, the discrete NLS equation (2.1) is equivalent to the dynamical system $\frac{d\mathbf{u}}{dt} = J\nabla H[\mathbf{u}]$, where $H[\mathbf{u}] : X \mapsto \mathbb{R}^1$ is the Hamiltonian function (2.2) and (J, ∇) are the standard symplectic and gradient operators, respectively. Operators (J, ∇) are block-diagonal with the 2-block at the node $n \in \mathbb{Z}^3$ being

$$J_n = \begin{bmatrix} 0 & 1 \\ -1 & 0 \end{bmatrix}, \qquad \nabla_n = \begin{bmatrix} \partial_{\mathrm{Re}(u_n)} \\ \partial_{\mathrm{Im}(u_n)} \end{bmatrix}$$

We consider the time-periodic (stationary) solutions of the discrete NLS equation (2.1) in the form

$$u_n(t) = \phi_n e^{i(1-6\epsilon)t}, \qquad n \in \mathbb{Z}^3, \;\; \phi_n \in \mathbb{C}, \tag{2.3}$$

where all parameters have been normalized for convenience. The sequence $\{\phi_n\}_{n\in\mathbb{Z}^3}$ is a solution of the difference equation

$$(1 - |\phi_n|^2)\phi_n = \epsilon\Sigma\phi_n, \qquad \Sigma = \Delta + 6, \qquad n \in \mathbb{Z}^3, \tag{2.4}$$

which is obtained by variation of the Lyapunov functional $\Lambda[\mathbf{u}] = H[\mathbf{u}] + Q[\mathbf{u}]$, such that the Euler–Lagrange equation $\nabla\Lambda[\mathbf{u}]|_{\mathbf{u}=\boldsymbol{\phi}} = 0$ is equivalent to the difference equation (2.4).

If the localized solution $\boldsymbol{\phi}$ of the difference equation (2.4) exists, the time-evolution of the discrete NLS lattice (2.1) near the time-periodic space-localized solution (2.3) is defined by the linearization

$$u_n(t) = e^{i(1-6\epsilon)t}\left(\phi_n + a_n e^{\lambda t} + \bar{b}_n e^{\bar{\lambda} t}\right), \qquad n \in \mathbb{Z}^3, \tag{2.5}$$

where λ is the spectral parameter and the sequence $\{(a_n, b_n)\}_{n\in\mathbb{Z}^3}$ solves the linear eigenvalue problem for difference operators

$$\left(1 - 2|\phi_n|^2\right) a_n - \phi_n^2 b_n - \epsilon\Sigma a_n = i\lambda a_n, \;\; -\bar{\phi}_n^2 a_n + \left(1 - 2|\phi_n|^2\right) b_n - \epsilon\Sigma b_n = -i\lambda b_n, \quad n \in \mathbb{Z}^3. \tag{2.6}$$

If there exists a solution with $\mathrm{Re}(\lambda) > 0$, the stationary solution (2.3) is called *spectrally unstable*. Otherwise, it is neutrally spectrally stable.

The difference equation (2.4) with $\epsilon = 0$ has a general set of localized modes on $n \in \mathbb{Z}^3$:

$$\phi_n^{(0)} = \begin{cases} e^{i\theta_n}, & n \in S, \\ 0, & n \in S^{\perp}, \end{cases} \tag{2.7}$$

where S is a bounded set of nodes on the lattice $n \in \mathbb{Z}^3$, $S^{\perp} = \mathbb{Z}^3 \backslash S$, and $\{\theta_n\}_{n \in S}$ is a set of phase configurations. The set $\{\theta_n\}_{n \in S}$ is arbitrary for $\epsilon = 0$. It is called a *vortex configuration* if $\theta_{n_0} = 0$ for a single node $n_0 \in S \subset \mathbb{Z}^3$ and $\theta_{n_1} \neq \{0, \pi\}$ for at least one $n_1 \in S$, $n_1 \neq n_0$. If $\theta_n \in \{0, \pi\}$, $\forall n \in S$, it is dubbed a *discrete soliton*. We address here the main questions: *For what vortex configurations, the localized mode (2.7) can be continued in the difference equation (2.4) for small $\epsilon > 0$ and is stable in the linearized discrete NLS equation (2.6)?*

Although the questions and the algorithms of their solution are rather general, we would like to consider specific vortex configurations in the three-dimensional NLS lattice. Some of these configurations have been addressed in the previous works [20, 21] as they are thought to be elementary building blocks of three-dimensional discrete structures. The three specific configurations are formulated in terms of the limiting solution (2.7).

(i) *A simple cube* consists of two adjacent planes of aligned vortex cells. More precisely, we set $S = S_0 \oplus S_1$, where

$$S_l = \{(0,0,l), (1,0,l), (1,1,l), (0,1,l)\}, \qquad l = 0, 1, \tag{2.8}$$

such that $N = \dim(S) = 8$. Let j be the index enumerating nodes in the contours S_0 and S_1 according to the order (2.8). Let $\theta_{l,j}$ be the corresponding phase in the set $\{\theta_n\}_{n \in S}$, where $l = 0, 1$ and $j = 1, 2, 3, 4$. Then, the simple cube vortex configurations are

$$\theta_{0,j} = \frac{\pi(j-1)}{2}, \qquad \theta_{1,j} = \theta_0 + s_0 \frac{\pi(j-1)}{2}, \qquad j = 1, 2, 3, 4, \tag{2.9}$$

where $\theta_0 = \{0, \frac{\pi}{2}, \pi, \frac{3\pi}{2}\}$ and $s_0 = \{+1, -1\}$. Two configurations with $s_0 = -1$ are redundant: the case $\theta_0 = \pi$ can be obtained from the case $\theta_0 = 0$ by multiplication of u_n by i and so does the case $\theta_0 = \frac{3\pi}{2}$ from the case $\theta_0 = \frac{\pi}{2}$. In what follows, we only consider the six irreducible vortex configurations and show that only three configurations persist for $\epsilon \neq 0$ and only one configuration with $\theta_0 = \pi$ and $s_0 = 1$ is linearly stable.

(ii) *A double cross* consists of two symmetric planes of aligned vortex crosses separated by an empty plane. More precisely, we set $S = S_{-1} \oplus S_1$, where

$$S_l = \{(-1,0,l), (0,-1,l), (1,0,l), (0,1,l)\}, \qquad l = -1, 1, \tag{2.10}$$

such that $N = \dim(S) = 8$. By using the same convention as in (i), the double cross vortex configurations are expressed by

$$\theta_{-1,j} = \frac{\pi(j-1)}{2}, \qquad \theta_{1,j} = \theta_0 + s_0 \frac{\pi(j-1)}{2}, \qquad j = 1, 2, 3, 4, \tag{2.11}$$

where $\theta_0 = \{0, \frac{\pi}{2}, \pi, \frac{3\pi}{2}\}$ and $s_0 = \{+1, -1\}$. Similarly to the simple cube vortex configurations, we will consider six irreducible vortex configurations and show that three configurations persist for $\epsilon \neq 0$ and only one configuration with $\theta_0 = \pi$ and $s_0 = 1$ is linearly stable.

(iii) *A diamond* consists of a quadrupole in a central plane, surrounded by two symmetric central off-plane nodes. More precisely, we set $S = S_{-1} \oplus S_0 \oplus S_1$, where

$$S_0 = \{(-1,0,0),(0,-1,0),(1,0,0),(0,1,0)\}, \qquad S_{\pm 1} = \{(0,0,\pm 1)\}, \tag{2.12}$$

such that $N = \dim(S) = 6$. By using the same convention as in (i), the diamond vortex configurations are expressed by

$$\theta_{0,j} = \pi(j-1), \qquad j = 1,2,3,4, \qquad \theta_{\pm 1,0} = \theta_0^{\pm}, \tag{2.13}$$

where $\theta_0^{\pm} = \{0, \frac{\pi}{2}, \pi, \frac{3\pi}{2}\}$. Six configurations with $\theta_0^- > \theta_0^+$ are redundant as they can be obtained from the corresponding configurations with $\theta_0^- < \theta_0^+$ by reflection: $\theta_0^{\pm} \mapsto \theta_0^{\mp}$. Three other configurations with $\theta_0^- = \theta_0^+ = \{\pi, \frac{3\pi}{2}\}$ and $\theta_0^- = \pi$, $\theta_0^+ = \frac{3\pi}{2}$ can be obtained from the configurations $\theta_0^- = \theta_0^+ = \{0, \frac{\pi}{2}\}$ and $\theta_0^- = 0$, $\theta_0^+ = \frac{\pi}{2}$ by multiplication of u_n by -1. One more configuration with $\theta_0^- = 0$ and $\theta_0^+ = \frac{3\pi}{2}$ can be obtained from the configuration with $\theta_0^- = 0$ and $\theta_0^+ = \frac{\pi}{2}$ by complex conjugation. In what follows, we only consider the six irreducible vortex configurations and show that only three configurations persist for $\epsilon \neq 0$ and only one configurations with $\theta_0^- = \frac{\pi}{2}$ and $\theta_0^+ = \frac{3\pi}{2}$ is stable.

3 Review of the Lyapunov–Schmidt reduction algorithm

We review the main results of [18], where the Lyapunov–Schmidt reduction method is developed to answer the questions outlined in Section 2.

Let $\mathcal{O}(0)$ be a small neighborhood of $\epsilon = 0$ on $\mathbb{R}^1$. Let $N = \dim(S)$ and $\mathcal{T}$ be the torus on $[0, 2\pi]^N$ for the vector $\boldsymbol{\theta}$ of phase components $\{\theta_n\}_{n \in S}$. We define the nonlinear vector field $\mathbf{F}(\boldsymbol{\phi}, \epsilon)$ on $\boldsymbol{\phi} \in X$ and $\epsilon \in \mathbb{R}^1$, such that the 2-block at the node $n \in \mathbb{Z}$ is written by

$$\mathbf{F}_n(\boldsymbol{\phi}, \epsilon) = \begin{bmatrix} (1 - |\phi_n|^2)\phi_n - \epsilon \Sigma \phi_n \\ (1 - |\phi_n|^2)\bar{\phi}_n - \epsilon \Sigma \bar{\phi}_n \end{bmatrix}. \tag{3.1}$$

The Jacobian $D_{\boldsymbol{\phi}} \mathbf{F}(\boldsymbol{\phi}, \epsilon)$ of the nonlinear vector field $\mathbf{F}(\boldsymbol{\phi}, \epsilon)$ at the solution $\boldsymbol{\phi}$ for each $\epsilon \in \mathcal{O}(0)$ coincides with the *linearized energy operator* $\mathcal{H}$ related to the quadratic form for the Lyapunov function $\Lambda[\mathbf{u}] = H[\mathbf{u}] + Q[\mathbf{u}]$ such that

$$\Lambda[\mathbf{u}] = \Lambda[\boldsymbol{\phi}] + \frac{1}{2}(\boldsymbol{\psi}, \mathcal{H}\boldsymbol{\psi}) + \mathrm{O}(\|\boldsymbol{\psi}\|^3_{X \times X}),$$

where $\mathbf{u}$ is expressed by (2.5) and the 2-block of $\boldsymbol{\psi} \in X \times X$ is defined at the node $n \in \mathbb{Z}^3$ by

$$\boldsymbol{\psi}_n = \begin{bmatrix} a_n \\ b_n \end{bmatrix}.$$

The matrix operator $\mathcal{H}$ on $\boldsymbol{\psi} \in X \times X$ is not block-diagonal due to the presence of the shift operator Σ. We can still use a formal notation $\mathcal{H}_n$ for the "2-block" of $\mathcal{H}$ at the node $n \in \mathbb{Z}^3$

$$\mathcal{H}_n = \begin{pmatrix} 1 - 2|\phi_n|^2 & -\phi_n^2 \\ -\bar{\phi}_n^2 & 1 - 2|\phi_n|^2 \end{pmatrix} - \epsilon \left(s_{+e_1} + s_{-e_1} + s_{+e_2} + s_{-e_2} + s_{+e_3} + s_{-e_3}\right) \begin{pmatrix} 1 & 0 \\ 0 & 1 \end{pmatrix}, \tag{3.2}$$

where $s_{e_j} u_n = u_{n+e_j}$ for $\{e_1, e_2, e_3\} \in \mathbb{Z}^3$. This notation allows us to write the matrix-vector form $\mathcal{H}\boldsymbol{\psi}$ in the component form $\mathcal{H}_n \boldsymbol{\psi}_n$ at each node $n \in \mathbb{Z}^3$. In particular, the linear eigenvalue problem (2.6) can be rewritten in the matrix-vector form

$$\sigma \mathcal{H} \boldsymbol{\psi} = i\lambda \boldsymbol{\psi}, \tag{3.3}$$

where the 2-block of σ is a diagonal matrix of $(1, -1)$ at each node $n \in \mathbb{Z}^3$.

Let $\boldsymbol{\phi}^{(0)} = \boldsymbol{\phi}^{(0)}(\boldsymbol{\theta})$ be the solution (2.7). By explicit computations, we have $\mathbf{F}(\boldsymbol{\phi}^{(0)}, 0) = \mathbf{0}$ and $\text{Ker}(\mathcal{H}^{(0)}) = \text{Span}(\{\mathbf{e}_n\}_{n \in S}) \subset X \times X$, where $\mathcal{H}^{(0)} = D_{\boldsymbol{\phi}} \mathbf{F}(\boldsymbol{\phi}^{(0)}, 0)$ is block-diagonal with the 2-block at the node $n \in \mathbb{Z}^3$ given by

$$(\mathcal{H}^{(0)})_n = \begin{bmatrix} 1 & 0 \\ 0 & 1 \end{bmatrix}, \ n \in S^{\perp}, \qquad (\mathcal{H}^{(0)})_n = \begin{bmatrix} -1 & -e^{2i\theta_n} \\ -e^{-2i\theta_n} & -1 \end{bmatrix}, \ n \in S.$$

We note that $\mathcal{H}^{(0)} \mathbf{e}_n = \mathbf{0}$ and $\mathcal{H}^{(0)} \hat{\mathbf{e}}_n = -2\hat{\mathbf{e}}_n$, $n \in S \subset \mathbb{Z}^3$, where the 2-blocks of eigenvectors $\mathbf{e}_n$ and $\hat{\mathbf{e}}_n$ at the node $k \in \mathbb{Z}^3$ are given by

$$(\mathbf{e}_n)_k = i \begin{bmatrix} e^{i\theta_n} \\ -e^{-i\theta_n} \end{bmatrix} \delta_{k,n}, \qquad (\hat{\mathbf{e}}_n)_k = \begin{bmatrix} e^{i\theta_n} \\ e^{-i\theta_n} \end{bmatrix} \delta_{k,n},$$

with $\delta_{k,n}$ being a standard Kroneker symbol. Let $\mathcal{P} : X \times X \mapsto \text{Ker}(\mathcal{H}^{(0)})$ be an orthogonal projection operator to the N-dimensional kernel of $\mathcal{H}^{(0)}$. In the explicit form, the projection operator $\mathcal{P}$ is expressed by

$$\forall \mathbf{f} = (\mathbf{f}_1, \mathbf{f}_2) \in X \times X : \qquad (\mathcal{P}\mathbf{f})_n = \frac{(\mathbf{e}_n, \mathbf{f})}{(\mathbf{e}_n, \mathbf{e}_n)} = \frac{1}{2i} \left(e^{-i\theta_n} (\mathbf{f}_1)_n - e^{i\theta_n} (\mathbf{f}_2)_n \right), \qquad n \in S. \tag{3.4}$$

We note that the constraint $\mathbf{f}_2 = \bar{\mathbf{f}}_1$ is added when solutions of the nonlinear vector equation $\mathbf{F}(\boldsymbol{\phi}, \epsilon) = \mathbf{0}$ are considered with $\boldsymbol{\phi} \in X$ and $\bar{\boldsymbol{\phi}} \in X$.

Since the operator $\mathcal{H}^{(0)}$ is a self-adjoint Fredholm operator of zero index, the decomposition $X \times X = \text{Ker}(\mathcal{H}^{(0)}) \oplus \text{Range}(\mathcal{H}^{(0)})$ is well-defined and so is the projection operator $(\mathcal{I} - \mathcal{P}) : X \times X \mapsto \text{Range}(\mathcal{H}^{(0)})$. By using the Lyapunov–Schmidt reduction algorithm, we consider the decomposition

$$\boldsymbol{\phi} = \boldsymbol{\phi}^{(0)}(\boldsymbol{\theta}) + \sum_{n \in S} \alpha_n \mathbf{e}_n + \boldsymbol{\varphi} \in X, \tag{3.5}$$

where $(\boldsymbol{\varphi}, \bar{\boldsymbol{\varphi}}) \in \text{Range}(\mathcal{H}^{(0)})$ and $\alpha_n \in \mathbb{R}$ for each $n \in S$. We note that

$$\forall \boldsymbol{\theta}_0 \in \mathcal{T} : \quad \boldsymbol{\phi}^{(0)}(\boldsymbol{\theta}_0) + \sum_{n \in S} \alpha_n \mathbf{e}_n = \boldsymbol{\phi}^{(0)}(\boldsymbol{\theta}_0 + \boldsymbol{\alpha}) + \text{O}(\|\boldsymbol{\alpha}\|^2_{\mathbb{R}^n}). \tag{3.6}$$

Since the values of $\boldsymbol{\theta}$ in $\boldsymbol{\phi}^{(0)}(\boldsymbol{\theta})$ have not been defined yet, we can set $\alpha_n = 0$, $\forall n \in S$ without loss of generality. The splitting equations in the Lyapunov–Schmidt reduction algorithm are

$$\mathcal{P}\mathbf{F}(\boldsymbol{\phi}^{(0)}(\boldsymbol{\theta}) + \boldsymbol{\varphi}, \epsilon) = 0, \qquad (\mathcal{I} - \mathcal{P})\mathbf{F}(\boldsymbol{\phi}^{(0)}(\boldsymbol{\theta}) + \boldsymbol{\varphi}, \epsilon) = 0.$$

We note that $(\mathcal{I} - \mathcal{P})\mathcal{H}(\mathcal{I} - \mathcal{P}) : \text{Range}(\mathcal{H}^{(0)}) \mapsto \text{Range}(\mathcal{H}^{(0)})$ is analytic in $\epsilon \in \mathcal{O}(0)$ and invertible at $\epsilon = 0$, while $\mathbf{F}(\boldsymbol{\phi}, \epsilon)$ is analytic in $\epsilon \in \mathcal{O}(0)$. By the Implicit Function Theorem for Analytic Vector Fields, there exists a unique solution $\boldsymbol{\varphi} \in X$ analytic in $\epsilon \in \mathcal{O}(0)$ and dependent on $\boldsymbol{\theta} \in \mathcal{T}$, such

that $\boldsymbol{\varphi} \equiv \boldsymbol{\varphi}(\boldsymbol{\theta}, \epsilon)$ and $\|\boldsymbol{\varphi}\|_X = \mathrm{O}(\epsilon)$ as $\epsilon \to 0$. As a result, there exists the nonlinear vector field $\mathbf{g} : \mathcal{T} \times \mathbb{R}^1 \mapsto \mathbb{R}^N$, such that the Lyapunov–Schmidt bifurcation equations are

$$\mathbf{g}(\boldsymbol{\theta}, \epsilon) = \mathcal{P}\mathbf{F}(\boldsymbol{\phi}^{(0)}(\boldsymbol{\theta}) + \boldsymbol{\varphi}(\boldsymbol{\theta}, \epsilon), \epsilon) = 0. \tag{3.7}$$

By the construction, the function $\mathbf{g}(\boldsymbol{\theta}, \epsilon)$ is analytic in $\epsilon \in \mathcal{O}(0)$ and $\mathbf{g}(\boldsymbol{\theta}, 0) = \mathbf{0}$ for any $\boldsymbol{\theta} \in \mathcal{T}$, such that the Taylor series for $\mathbf{g}(\boldsymbol{\theta}, \epsilon)$ in $\epsilon \in \mathcal{O}(0)$ is given by

$$\mathbf{g}(\boldsymbol{\theta}, \epsilon) = \sum_{k=1}^{\infty} \epsilon^k \mathbf{g}^{(k)}(\boldsymbol{\theta}). \tag{3.8}$$

By the gauge symmetry, the function $\mathbf{g}(\boldsymbol{\theta}, \epsilon)$ satisfies the following relation:

$$\forall \alpha_0 \in \mathbb{R}^1, \ \ \forall \boldsymbol{\theta} \in \mathcal{T} : \qquad \mathbf{g}(\boldsymbol{\theta} + \alpha_0 \mathbf{p}_0, \epsilon) = \mathbf{g}(\boldsymbol{\theta} + \alpha_0 \mathbf{p}_0, \epsilon), \tag{3.9}$$

where $\mathbf{p}_0 = (1, 1, ..., 1)^T \in \mathbb{R}^N$. The main theorem of the Lyapunov–Schmidt reduction algorithm is summarized as follows:

Theorem 1 (Persistence) *The configuration $\boldsymbol{\phi}^{(0)}(\boldsymbol{\theta})$ in (2.7) can be continued to the domain $\epsilon \in \mathcal{O}(0)$ if and only if there exists a root $\boldsymbol{\theta}_* \in \mathcal{T}$ of the vector field $\mathbf{g}(\boldsymbol{\theta}, \epsilon)$ in (3.7). Moreover, if the root $\boldsymbol{\theta}_*$ is analytic in $\epsilon \in \mathcal{O}(0)$ and $\boldsymbol{\theta}_* = \boldsymbol{\theta}_0 + \mathrm{O}(\epsilon)$, the solution $\boldsymbol{\phi}$ of the difference equation (2.4) is analytic in $\epsilon \in \mathcal{O}(0)$, such that*

$$\boldsymbol{\phi} = \boldsymbol{\phi}^{(0)}(\boldsymbol{\theta}_*) + \boldsymbol{\varphi}(\boldsymbol{\theta}_*, \epsilon) = \boldsymbol{\phi}^{(0)}(\boldsymbol{\theta}_0) + \sum_{k=1}^{\infty} \epsilon^k \boldsymbol{\phi}^{(k)}(\boldsymbol{\theta}_0), \tag{3.10}$$

where $\boldsymbol{\phi}^{(k)}(\boldsymbol{\theta}_0)$, $k \in \mathbb{N}$ are independent on ϵ.

Implementation of the Lyapunov–Schmidt reduction algorithm is based on the analysis of the convergent Taylor series expansions (3.8) and (3.10). Let $\mathcal{M} = D_{\boldsymbol{\theta}} \mathbf{g}(\boldsymbol{\theta}, \epsilon) : \mathbb{R}^N \mapsto \mathbb{R}^N$ be the Jacobian matrix evaluated at the vector $\boldsymbol{\theta} \in \mathcal{T}$. By the symmetry of the shift operators Σ, the matrix $\mathcal{M}$ is symmetric. By the gauge transformation (3.9), $\mathcal{M}\mathbf{p}_0 = \mathbf{0} \in \mathbb{R}^N$, such that the spectrum of $\mathcal{M}$ includes a zero eigenvalue. If the zero eigenvalue of $\mathcal{M}$ is simple, zeros $\boldsymbol{\theta}_*$ of the function $\mathbf{g}(\boldsymbol{\theta}, \epsilon)$ are uniquely continued in ϵ modulo the gauge transformation (3.9) by using the Implicit Function Theorem for Analytic Vector Fields.

Algorithm 1 (Persistence) *Suppose that $\mathbf{g}^{(k)}(\boldsymbol{\theta}) \equiv \mathbf{0}$ for $k = 1, 2, ..., \kappa - 1$ and $\mathbf{g}^{(\kappa)}(\boldsymbol{\theta}) \neq \mathbf{0}$ for $\kappa \geq 1$. Let $\boldsymbol{\theta}_0$ be the root of $\mathbf{g}^{(\kappa)}(\boldsymbol{\theta})$ and $\mathcal{M}^{(k)} = D_{\boldsymbol{\theta}} \mathbf{g}^{(k)}(\boldsymbol{\theta}_0)$ for $k \geq \kappa$.*

1. *If $\mathrm{Ker}(\mathcal{M}^{(\kappa)}) = \mathrm{Span}(\mathbf{p}_0) \subset \mathbb{R}^N$, then the configuration (2.7) is uniquely continued in $\epsilon \in \mathcal{O}(0)$ modulo the gauge transformation (3.9).*
2. *Let $\mathrm{Ker}(\mathcal{M}^{(\kappa)}) = \mathrm{Span}(\mathbf{p}_0, \mathbf{p}_1, ..., \mathbf{p}_{d_\kappa}) \subset \mathbb{R}^N$ with $1 \leq d_\kappa \leq N - 1$ and $P^{(\kappa)} : \mathbb{R}^N \mapsto \mathrm{Ker}(\mathcal{M}^{(\kappa)})$ be the projection matrix. Then,*
   (a) *If $\mathbf{g}^{(\kappa+1)}(\boldsymbol{\theta}_0) \notin \mathrm{Range}(\mathcal{M}^{(\kappa)})$, the configuration (2.7) does not persist for any $\epsilon \neq 0$.*

(b) If $\mathbf{g}^{(\kappa+1)}(\boldsymbol{\theta}_0) \in \text{Range}(\mathcal{M}^{(\kappa)})$*, the configuration (2.7) is continued to the next order. Replace*

$$\begin{aligned} \mathcal{M}^{(\kappa)} &\mapsto P^{(\kappa)}\mathcal{M}^{(\kappa+1)}P^{(\kappa)}, \\ P^{(\kappa)} &\mapsto P^{(\kappa+1)} : \mathbb{R}^N \mapsto \text{Ker}(P^{(\kappa)}\mathcal{M}^{(\kappa+1)}P^{(\kappa)}), \\ \boldsymbol{\theta}_0 &\mapsto \boldsymbol{\theta}_0 - \epsilon \left(\mathcal{M}^{(\kappa)}\right)^{-1} \mathbf{g}^{(\kappa+1)}(\boldsymbol{\theta}_0), \\ \mathbf{g}^{(k+1)} &\mapsto \mathbf{g}^{(k+2)} \end{aligned}$$

and repeat the previous two steps.

If the algorithm stops at the order K *with* $\kappa \leq K < \infty$*, conclude whether the vortex configuration continues in* ϵ *or terminates at* $\epsilon = 0$*. If no* $K < \infty$ *exists, the algorithm does not converge in a finite number of iterations.*

Few remarks regarding Algorithm 1 are in place. For subsequent iterations of the algorithm, one needs to extend the power series

$$\boldsymbol{\theta}_* = \boldsymbol{\theta}_0 - \epsilon \left(\mathcal{M}^{(\kappa)}\right)^{-1} \mathbf{g}^{(\kappa+1)}(\boldsymbol{\theta}_0) + \text{O}(\epsilon^2) \tag{3.11}$$

to higher orders of ϵ. This expansion is evaluated from the Taylor series (3.8). Additionally, the situation when the algorithm does not converge in a finite number of iterations may imply that the particular vortex configuration persists beyond all orders of ϵ and has additional parameters besides the parameter α_0 in the gauge transformation (3.9).

If the algorithm converges in a finite number of iterations, it provides a binary answer on whether the configuration persists beyond $\epsilon \neq 0$ or terminates at $\epsilon = 0$. Simultaneously, the method enables us to predict spectral stability of the persistent vortex configurations. To consider stability of vortex configurations, we need to consider the spectrum of operators $\mathcal{H}$ and $\sigma\mathcal{H}$ in the neighborhood of the zero eigenvalue for $\epsilon \in \mathcal{O}(0)$.

Using the representation (3.2) and the Taylor series expansion (3.10), we represent operator $\mathcal{H}$ by its Taylor series

$$\mathcal{H} = \mathcal{H}^{(0)} + \sum_{k=1}^{\infty} \epsilon^k \mathcal{H}^{(k)} \tag{3.12}$$

and consider the truncated eigenvalue problem for the spectrum of $\mathcal{H}$:

$$\left[\mathcal{H}^{(0)} + \epsilon\mathcal{H}^{(1)} + ... + \epsilon^{k-1}\mathcal{H}^{(k-1)} + \epsilon^k\mathcal{H}^{(k)} + \text{O}(\epsilon^{k+1})\right]\boldsymbol{\psi} = \mu\boldsymbol{\psi},$$

where μ is eigenvalue and $\boldsymbol{\psi} \in X \times X$ is an eigenvector.

Let $\boldsymbol{\alpha} \in \text{Ker}(\mathcal{M}^{(\kappa)}) \cap \text{Ker}(\mathcal{M}^{(\kappa+1)}) \cap ... \cap \text{Ker}(\mathcal{M}^{(k-1)}) \subset \mathbb{R}^N$ but $\boldsymbol{\alpha} \notin \text{Ker}(\mathcal{M}^{(k)})$ for some $\kappa \leq k \leq K$. It is clear that $\boldsymbol{\alpha}$ has $(d_{k-1}+1)$ arbitrary parameters, where $d_{\kappa-1} = N-1$. By using the projection operator $\mathcal{P}$ in (3.4) and the relation (3.6), we obtain that

$$\boldsymbol{\alpha} = \mathcal{P}\left(\sum_{n\in S} \alpha_n \mathbf{e}_n\right), \qquad \left(\sum_{n\in S} \alpha_n \mathbf{e}_n\right) = D_{\boldsymbol{\theta}}\boldsymbol{\phi}^{(0)}(\boldsymbol{\theta}_0)\boldsymbol{\alpha},$$

where $D_{\boldsymbol{\theta}}\boldsymbol{\phi}^{(0)}(\boldsymbol{\theta}_0)$ is the Jacobian matrix of the infinite-dimensional vector $(\boldsymbol{\phi}^{(0)}(\boldsymbol{\theta}), \bar{\boldsymbol{\phi}}^{(0)}(\boldsymbol{\theta}))$ with respect to $\boldsymbol{\theta}^T$. It is clear that

$$\mathcal{H}^{(0)}\boldsymbol{\psi}^{(0)} = 0, \quad \text{where} \quad \boldsymbol{\psi}^{(0)} = \sum_{n\in S} \alpha_n \mathbf{e}_n = D_{\boldsymbol{\theta}}\boldsymbol{\phi}^{(0)}(\boldsymbol{\theta}_0)\boldsymbol{\alpha}.$$

Moreover, the partial $(k-1)$-th sum of the power series (3.10) gives the zero of the nonlinear vector field (3.1) up to the order $\mathrm{O}(\epsilon^k)$ and has $(d_{k-1}+1)$ arbitrary parameters when $\boldsymbol{\theta}_0$ is shifted in the direction of the vector $\boldsymbol{\alpha}$. At the tangent space of the nonlinear vector fields (3.1) in the direction of $\boldsymbol{\alpha}$, the linear inhomogeneous system

$$\mathcal{H}^{(0)}\boldsymbol{\psi}^{(m)} + \mathcal{H}^{(1)}\boldsymbol{\psi}^{(m-1)} + ... + \mathcal{H}^{(m)}\boldsymbol{\psi}^{(0)} = \mathbf{0}, \qquad m = 1, 2, ..., k-1$$

has a particular solution in the form $\boldsymbol{\psi}^{(m)} = D_{\boldsymbol{\theta}}\boldsymbol{\phi}^{(m)}(\boldsymbol{\theta}_0)\boldsymbol{\alpha}$ for $m = 1, 2, ..., k-1$. By extending the regular perturbation series for isolated zero eigenvalues of $\mathcal{H}^{(0)}$,

$$\boldsymbol{\psi} = \boldsymbol{\psi}^{(0)} + \epsilon\boldsymbol{\psi}^{(1)} + ... + \epsilon^k\boldsymbol{\psi}^{(k)} + \mathrm{O}(\epsilon^{k+1}), \qquad \mu = \mu_k\epsilon^k + \mathrm{O}(\epsilon^{k+1}), \tag{3.13}$$

we obtain the linear inhomogeneous equation

$$\mathcal{H}^{(0)}\boldsymbol{\psi}^{(k)} + \mathcal{H}^{(1)}\boldsymbol{\psi}^{(k-1)} + ... + \mathcal{H}^{(k)}\boldsymbol{\psi}^{(0)} = \mu_k\boldsymbol{\psi}^{(0)}.$$

Applying the projection operator $\mathcal{P}$ and recalling the definition (3.7), we find that the left-hand-side of the linear equation reduces to the form

$$\mathcal{P}\left[\mathcal{H}^{(1)}D_{\boldsymbol{\theta}}\boldsymbol{\phi}^{(k-1)}(\boldsymbol{\theta}_0) + ... + \mathcal{H}^{(k)}D_{\boldsymbol{\theta}}\boldsymbol{\phi}^{(0)}(\boldsymbol{\theta}_0)\right]\boldsymbol{\alpha} = D_{\boldsymbol{\theta}}\mathbf{g}^{(k)}(\boldsymbol{\theta}_0)\boldsymbol{\alpha} = \mathcal{M}^{(k)}\boldsymbol{\alpha},$$

while $\mathcal{P}\boldsymbol{\psi}^{(0)} = \boldsymbol{\alpha}$. Therefore, μ_k is an eigenvalue of the Jacobian matrix $\mathcal{M}^{(k)}$ and $\boldsymbol{\alpha}$ is the corresponding eigenvector. The equivalence between non-zero small eigenvalues of $\mathcal{H}$ and non-zero eigenvalues of $\mathcal{M}$ is summarized as follows:

Theorem 2 (Eigenvalues of $\mathcal{H}$) *Let Algorithm 1 converge at the K-th order and the solution $\boldsymbol{\phi}$ in Theorem 1 persist for $\epsilon \neq 0$. Then,*

$$\lambda_{\neq 0}(P^{(m-1)}\mathcal{M}^{(m)}P^{(m-1)})\epsilon^m + \mathrm{O}(\epsilon^{m+1}) \quad \subset \quad \sigma(\mathcal{H}), \qquad m = \kappa, \kappa+1, ..., K,$$

where $\lambda_{\neq 0}(\mathcal{M})$ and $\sigma(\mathcal{H})$ denote non-zero eigenvalues of matrix $\mathcal{M}$ and spectrum of operator $\mathcal{H}$, and $P^{(\kappa-1)}$ is an identity operator.

Similarly to the computations of small non-zero eigenvalues of $\mathcal{H}$, we consider eigenvalues of the spectral problem (3.3) truncated at the k-th order approximation:

$$\left[\mathcal{H}^{(0)} + \epsilon\mathcal{H}^{(1)} + ... + \epsilon^{k-1}\mathcal{H}^{(k-1)} + \epsilon^k\mathcal{H}^{(k)} + \mathrm{O}(\epsilon^{k+1})\right]\boldsymbol{\psi} = i\lambda\sigma\boldsymbol{\psi}.$$

By using relations $\hat{\mathbf{e}}_n = -i\sigma\mathbf{e}_n$ and $\mathcal{H}^{(0)}\hat{\mathbf{e}}_n = -2\hat{\mathbf{e}}_n$, $\forall n \in S$, we can see that the linear inhomogeneous equation

$$\mathcal{H}^{(0)}\boldsymbol{\varphi}^{(0)} = 2i\sigma D_{\boldsymbol{\theta}}\boldsymbol{\phi}^{(0)}(\boldsymbol{\theta}_0)\boldsymbol{\alpha}$$

has a solution

$$\boldsymbol{\varphi}^{(0)} = \sum_{n \in S} \alpha_n \hat{\mathbf{e}}_n = \boldsymbol{\Phi}^{(0)}(\boldsymbol{\theta}_0)\boldsymbol{\alpha},$$

where $\boldsymbol{\Phi}^{(0)}(\boldsymbol{\theta}_0)$ is the matrix extension of $\boldsymbol{\phi}^{(0)}(\boldsymbol{\theta}_0)$, which consists of vector columns $\hat{\mathbf{e}}_n$, $n \in S$. Similarly, there exists a particular solution of the inhomogeneous problem

$$\mathcal{H}^{(0)}\boldsymbol{\varphi}^{(m)} + \mathcal{H}^{(1)}\boldsymbol{\varphi}^{(m-1)} + ... + \mathcal{H}^{(m)}\boldsymbol{\varphi}^{(0)} = 2i\sigma D_{\boldsymbol{\theta}}^T \boldsymbol{\phi}^{(m)}(\boldsymbol{\theta}_0)\boldsymbol{\alpha}, \qquad m = 1, 2, ..., k',$$

in the form $\boldsymbol{\varphi}^{(m)} = \boldsymbol{\Phi}^{(m)}(\boldsymbol{\theta}_0)\boldsymbol{\alpha}$, where $k' = (k-1)/2$ if k is odd and $k' = k/2 - 1$ if k is even. By extending the regular perturbation series for isolated zero eigenvalue of $\sigma\mathcal{H}^{(0)}$,

$$\boldsymbol{\psi} = \boldsymbol{\psi}^{(0)} + \epsilon\boldsymbol{\psi}^{(1)} + ... + \epsilon^{k-1}\boldsymbol{\psi}^{(k-1)} + \frac{1}{2}\lambda\left(\boldsymbol{\varphi}^{(0)} + \epsilon\boldsymbol{\varphi}^{(1)} + ... + \epsilon^{k'}\boldsymbol{\varphi}^{(k')}\right) + \epsilon^k\boldsymbol{\psi}^{(k)} + \mathrm{O}(\epsilon^{k+1}), \quad (3.14)$$

where $\boldsymbol{\psi}^{(m)} = D_{\boldsymbol{\theta}}\boldsymbol{\phi}^{(m)}(\boldsymbol{\theta}_0)\boldsymbol{\alpha}$ for $m = 0, 1, ..., k-1$, $\boldsymbol{\varphi}^{(m)} = \boldsymbol{\Phi}^{(m)}(\boldsymbol{\theta}_0)\boldsymbol{\alpha}$ for $m = 0, 1, .., k'$, and $\lambda = \epsilon^{k/2}\lambda_{k/2} + \mathrm{O}(\epsilon^{k/2+1})$, we obtain a linear inhomogeneous problem for $\boldsymbol{\psi}^{(k)}$ at the order $\mathrm{O}(\epsilon^k)$. When k is odd, the linear problem takes the form

$$\mathcal{H}^{(0)}\boldsymbol{\psi}^{(k)} + \mathcal{H}^{(1)}\boldsymbol{\psi}^{(k-1)} + ... + \mathcal{H}^{(k)}\boldsymbol{\psi}^{(0)} = \frac{i}{2}\lambda_{k/2}^2\sigma\boldsymbol{\varphi}^{(0)}. \quad (3.15)$$

When k is even,the linear problem takes the form

$$\mathcal{H}^{(0)}\boldsymbol{\psi}^{(k)} + \mathcal{H}^{(1)}\boldsymbol{\psi}^{(k-1)} + ... + \mathcal{H}^{(k)}\boldsymbol{\psi}^{(0)} + \frac{1}{2}\lambda_{k/2}\left(\mathcal{H}^{(1)}\boldsymbol{\varphi}^{(k')} + ... + \mathcal{H}^{(k'+1)}\boldsymbol{\varphi}^{(0)}\right) = \frac{i}{2}\lambda_{k/2}^2\sigma\boldsymbol{\varphi}^{(0)}. \quad (3.16)$$

By using the projection operator $\mathcal{P}$, we establish the equivalence between non-zero small eigenvalues of the operator $\sigma\mathcal{H}$ and non-zero eigenvalues of the reduced eigenvalue problems as follows:

Theorem 3 (Stability) *Let Algorithm 1 converge at the K-th order and the solution $\boldsymbol{\phi}$ in Theorem 1 persist for $\epsilon \neq 0$. Let operator $\mathcal{H}$ have a small eigenvalue μ of multiplicity d, such that $\mu = \epsilon^k\mu_k + \mathrm{O}(\epsilon^{k+1})$. Then, the eigenvalue problem (3.3) admits $(2d)$ small eigenvalues λ, such that $\lambda = \epsilon^{k/2}\lambda_{k/2} + \mathrm{O}(\epsilon^{k/2+1})$, where non-zero values $\lambda_{k/2}$ are found from the quadratic eigenvalue problems*

$$\textit{odd } k: \quad \mathcal{M}^{(k)}\boldsymbol{\alpha} = \frac{1}{2}\lambda_{k/2}^2\boldsymbol{\alpha}, \quad (3.17)$$

$$\textit{even } k: \quad \mathcal{M}^{(k)}\boldsymbol{\alpha} + \frac{1}{2}\lambda_{k/2}\mathcal{L}^{(k)}\boldsymbol{\alpha} = \frac{1}{2}\lambda_{k/2}^2\boldsymbol{\alpha}, \quad (3.18)$$

where $\mathcal{L}^{(k)} = \mathcal{P}\left[\mathcal{H}^{(1)}\boldsymbol{\Phi}^{(k')}(\boldsymbol{\theta}_0) + ... + \mathcal{H}^{(k'+1)}\boldsymbol{\Phi}^{(0)}(\boldsymbol{\theta}_0)\right]$.

We note that matrix $\mathcal{L}^{(k)}$ must be skew-symmetric so that all eigenvalues of the quadratic eigenvalue problem (3.18) occur in pairs $\lambda_{k/2}$ and $-\lambda_{k/2}$, which is a standard feature of linearized Hamiltonian dynamical systems. Computations of these eigenvalues can be achieved with a simple algorithm.

Algorithm 2 (Stability) *Suppose that the solution $\boldsymbol{\phi}$ persists in Algorithm 1 and compute $\mathcal{M}^{(k)} = D_{\boldsymbol{\theta}}\mathbf{g}^{(k)}(\boldsymbol{\theta}_0)$ for $\kappa \leq k \leq K$.*

1. *For each order k, where eigenvalues of $\mathcal{M}^{(k)}$ are non-zero, compute matrices $\mathcal{L}^{(k)}$.*

2. *Find roots $\lambda_{k/2}$ of the determinant equation for the quadratic eigenvalue problems (3.17)–(3.18).*

Example 1 Consider vortex configurations (2.9) on the simple cube (2.8). By explicit computations, the bifurcation equations are non-empty at the order $\kappa = 1$:

$$g_{l,j}^{(1)} = \sin(\theta_{l,j+1} - \theta_{l,j}) + \sin(\theta_{l,j-1} - \theta_{l,j}) + \sin(\theta_{l+1,j} - \theta_{l,j}), \qquad l = 0, 1, \quad j = 1, 2, 3, 4, \tag{3.19}$$

where $\theta_{2,j} = \theta_{0,j}$. Roots of $\mathbf{g}^{(1)}(\boldsymbol{\theta})$ occur for vortex configurations (2.9) with $\theta_0 = \{0, \pi\}$ and $s_0 = \{+1, -1\}$. The other vortex configurations (2.9) with $\theta_0 = \{\frac{\pi}{2}, \frac{3\pi}{2}\}$ and $s_0 = \{+1, -1\}$ terminate at $k = 1$ of Algorithm 1. The Jacobian matrix $\mathcal{M}^{(1)}$ has eigenvalue $\lambda_{\neq 0}(\mathcal{M}^{(1)}) = 2$ of multiplicity 4 for $\theta_0 = 0$ and $s_0 = 1$, eigenvalue $\lambda_{\neq 0}(\mathcal{M}^{(1)}) = -2$ of multiplicity 4 for $\theta_0 = \pi$ and $s_0 = 1$, and two eigenvalues $\lambda_{\neq 0}(\mathcal{M}^{(1)}) = \{-2, 2\}$ of multiplicity 2 for $\theta_0 = 0$ and $s_0 = -1$. (The same result holds for $\theta_0 = \pi$ and $s_0 = -1$ by symmetry.) Algorithm 1 does not converge at $k = 1$, since $\mathrm{Ker}(\mathcal{M}^{(1)})$ is four-dimensional in all cases. Our results described in Example 2 indicate that Algorithm 1 converges at the order $K = 6$ and the three vortex configurations above are uniquely continued in $\epsilon \in \mathrm{O}(0)$ modulo the gauge transformation (3.9).

4 Computations of vortex configurations

We have created the symbolic package that performs all steps of Algorithms 1 and 2 described in Section 3. The user is supposed to input the configuration of active nodes S and the corresponding set of angles $\{\theta_n\}_{n \in S}$. The package performs computations order by order to detect if the phase configuration persists in the Lyapunov–Schmidt reduction algorithm and if it is spectrally stable. For all configurations (i)–(iii) described in Section 2, we have found that Algorithm 1 terminates at the finite order $k = K < \infty$ and the persistent configurations have $\boldsymbol{\theta}_* = \boldsymbol{\theta}_0$ up to the order $k = K$, where $\boldsymbol{\theta}_0$ is the root of the first non-empty correction $\mathbf{g}^{(\kappa)}(\boldsymbol{\theta})$ with $\kappa \geq 1$.

The package consists of two parts. The first part performs computations of the correction terms $\mathbf{g}^{(k)}(\boldsymbol{\theta}_0)$ of the vector field $\mathbf{g}(\boldsymbol{\theta}, \epsilon)$ and the Jacobian matrices $\mathcal{M}^{(k)} = D_{\boldsymbol{\theta}} \mathbf{g}^{(k)}(\boldsymbol{\theta}_0)$ for a given vector $\boldsymbol{\theta}_0$ with $\kappa \leq k \leq K$ according to Algorithm 1. We have confirmed that there exists $K < \infty$ such that $\mathrm{dimKer}(\mathcal{M}^{(K)}) = 1$. We have also checked that $\mathbf{g}^{(k)}(\boldsymbol{\theta}_0) \equiv 0$, $\kappa \leq k \leq K$ for all persistent configurations, such that no extension of the series (3.11) is necessary. All non-persistent configurations terminate because $\mathbf{g}^{(\kappa)}(\boldsymbol{\theta}_0) \neq 0$, i.e. the given vortex configuration $\boldsymbol{\theta}_0$ is not a root of the first non-empty correction $\mathbf{g}^{(\kappa)}(\boldsymbol{\theta})$.

Non-zero eigenvalues of $\mathcal{M}^{(k)}$ are recorded in the first part of the package for $\kappa \leq k \leq K$. By Theorem 2, these non-zero eigenvalues give approximations of the small eigenvalues of the linearized Hamiltonian $\mathcal{H}$ at the order of $\mathrm{O}(\epsilon^k)$. The second part of the package performs computations of eigenvalues of the quadratic eigenvalue problems (3.17)–(3.18) according to Algorithm 2. Finding roots of the relevant determinant equations is not computationally difficult because the quadratic problem (3.17) is diagonal in λ^2 and the quadratic problem (3.18) is given typically by a matrix of small size.

Example 2 Continuing Example 1, we have found four non-zero eigenvalues of $\mathcal{M}^{(1)}$ at each persistent configuration, which result in four pairs of small eigenvalues $\lambda_{1/2}$ of the quadratic problem (3.17). For

instance, the vortex configuration (2.9) with $\theta_0 = \pi$ and $s_0 = 1$ has $\lambda_{\neq 0}(\mathcal{M}^{(1)}) = -2$ of multiplicity 4 and a pair of eigenvalues $\lambda_{1/2} = \pm\sqrt{2\lambda_{\neq 0}(\mathcal{M}^{(1)})} = \pm 2i$ of multiplicity 4. Continuing Algorithms 1 and 2 to the order $k = 2$, we find two non-zero eigenvalues of $P^{(1)}\mathcal{M}^{(2)}P^{(1)}$, which result in two pairs of small eigenvalues λ_1 of the quadratic problem (3.18) with a non-zero matrix $\mathcal{L}^{(2)}$. For the same selected configuration, these eigenvalues are $\lambda_{\neq 0}(\mathcal{M}_2) = 2$ of multiplicity 2 and a pair of eigenvalues $\lambda_1 = \pm 2i$ of multiplicity 2. Continuing the algorithm, we have found no non-zero eigenvalues for matrices $P^{(2)}\mathcal{M}^{(3,4,5)}P^{(2)}$ and the last non-zero eigenvalue for the matrix $P^{(2)}\mathcal{M}^{(6)}P^{(2)}$, such that $K = 6$. The non-zero eigenvalue of $P^{(2)}\mathcal{M}^{(6)}P^{(2)}$ results in a pair of small eigenvalues λ_3 of the quadratic problem (3.18), where the matrix $\mathcal{L}^{(6)}$ was found to be identically zero. For the same selected configuration, the last non-zero eigenvalue is $\lambda_{\neq 0}(\mathcal{M}^{(6)}) = -16$ and a pair of simple eigenvalues is $\lambda_3 = \pm\sqrt{2\lambda_{\neq 0}(\mathcal{M}^{(6)})} = \pm 4\sqrt{2}i$. The two parts of the output of the symbolic computational package for the selected vortex configuration are reproduced in Appendix A from the outputs of the Mathematica software package.

Similar to Example 2, we have performed computations of all configurations (i)–(iii) listed in Section 2. Our results are summarized in Tables 1–3 where we use the following convention: the entry 2×4 on the first line of Table 1 denotes the non-zero eigenvalue 2 of algebraic multiplicity 4 for a persistent vortex configuration. The binary conclusions on persistence and stability of the given vortex configuration are also listed for the reader's convenience.

Table 1: Vortex configurations (2.9) on the simple cube (2.8)

S_1	Persists	Eigenvalues of $\mathcal{H}$			Eigenvalues of $i\sigma\mathcal{H}$			Stable
		ϵ	ϵ^2	ϵ^6	$\epsilon^{1/2}$	ϵ	ϵ^3	
$\{0, \frac{\pi}{2}, \pi, \frac{3\pi}{2}\}$	Yes	$\{2 \times 4\}$	$\{2 \times 2\}$	$\{-16\}$	$\{\pm 2 \times 4\}$	$\{\pm 2i \times 2\}$	$\{\pm 4i\sqrt{2}\}$	No
$\{0, \frac{3\pi}{2}, \pi, \frac{\pi}{2}\}$	Yes	$\{-2 \times 2, 2 \times 2\}$	$\{2 \times 2\}$	$\{-16\}$	$\{\pm 2 \times 2, \pm 2i \times 2\}$	$\{\pm 2 \times 2\}$	$\{\pm 4i\sqrt{2}\}$	No
$\{\frac{\pi}{2}, \pi, \frac{3\pi}{2}, 0\}$	No							
$\{\frac{\pi}{2}, 0, \frac{3\pi}{2}, \pi\}$	No							
$\{\pi, \frac{3\pi}{2}, 0, \frac{\pi}{2}\}$	Yes	$\{-2 \times 4\}$	$\{2 \times 2\}$	$\{-16\}$	$\{\pm 2i \times 4\}$	$\{\pm 2i \times 2\}$	$\{\pm 4i\sqrt{2}\}$	Yes
$\{\frac{3\pi}{2}, 0, \frac{\pi}{2}, \pi\}$	No							

Table 2: Vortex configurations (2.11) on the double cross (2.10)

S_1	Persists	Eigenvalues of $\mathcal{H}$		Eigenvalues of $i\sigma\mathcal{H}$		Stable
		ϵ^2	ϵ^4	ϵ	ϵ^2	
$\{0, \frac{\pi}{2}, \pi, \frac{3\pi}{2}\}$	Yes	$\{-2 \times 2, 2 \times 2\}$	$\{-8, 28 \times 2\}$	$\{\pm 2 \times 2, \pm 2i \times 2\}$	$\{\pm 4i, \pm 2\sqrt{14} \times 2\}$	No
$\{0, \frac{3\pi}{2}, \pi, \frac{\pi}{2}\}$	Yes	$\{-4, -2 \times 3, 2\}$	$\{-8, 28\}$	$\{\pm 2, \pm 2i \times 3, \pm 2i\sqrt{2}\}$	$\{\pm 4i, \pm 2\sqrt{14}\}$	No
$\{\frac{\pi}{2}, \pi, \frac{3\pi}{2}, 0\}$	No					
$\{\frac{\pi}{2}, 0, \frac{3\pi}{2}, \pi\}$	No					
$\{\pi, \frac{3\pi}{2}, 0, \frac{\pi}{2}\}$	Yes	$\{-4 \times 2, -2 \times 4\}$	$\{-8\}$	$\{\pm 2i \times 4, \pm 2i\sqrt{2} \times 2\}$	$\{\pm 4i\}$	Yes
$\{\frac{3\pi}{2}, 0, \frac{\pi}{2}, \pi\}$	No					

Table 3: Configurations (2.13) on the diamond (2.12)

S_{-1}	S_1	Persists	Eigenvalues of $\mathcal{H}$		Eigenvalues of $i\sigma\mathcal{H}$		Stable
			ϵ^2	ϵ^4	ϵ	ϵ^2	
0	0	Yes	$\{-12, -6, 2, 2, 4\}$		$\{\pm 2 \times 2, \pm 2\sqrt{2}, \pm 2i\sqrt{3}, \pm 2i\sqrt{6}\}$		No
0	$\frac{\pi}{2}$	No					
0	π	Yes	$\{-2 \times 2, -5 \pm \sqrt{41}\}$	12	$\{\pm 2i \times 2, \pm\sqrt{-10 + 2\sqrt{41}}, \pm i\sqrt{10 + 2\sqrt{41}}\}$	$\pm 2\sqrt{6}$	No
$\frac{\pi}{2}$	$\frac{\pi}{2}$	No					
$\frac{\pi}{2}$	π	No					
$\frac{\pi}{2}$	$\frac{3\pi}{2}$	Yes	$\{-8, -2 \times 3\}$	-12	$\{\pm 2i \times 3, \pm 4i\}$	$\pm 2i\sqrt{6}$	Yes

5 Comparison with full eigenvalue computations

We proceed to test the predictions of the symbolic computations against the results of direct numerical approximations of relevant configurations and associated eigenvalues. Starting from the anti-continuum limit where the solutions (2.7) are explicit, we use numerical continuation techniques to obtain the corresponding solutions of the difference equations (2.4) for finite coupling strengths of $\epsilon < 0.2$. Numerical approximations of the vortex solutions are obtained with the fixed point iterations using Newton's method. Once the solution $\{\phi_n\}_{n\in\mathbb{Z}^3}$ is obtained to the desired numerical accuracy (typically 10^{-8}) on a truncated numerical domain, the eigenvalue problem (2.6) becomes a large matrix eigenvalue problem, which is fully solved using standard numerical algebra tools. The relevant eigenvalues with small real and imaginary parts are isolated and their dependence on ϵ is accordingly extracted and compared to the theoretical predictions of Tables 1–3. The results are shown in Figures 1-9, which are discussed in more detail below. In general, we denote numerically computed eigenvalues by solid (blue) lines, while their counterparts from symbolic computations are plotted by dashed (red) lines. Pairs of multiple real or imaginary eigenvalues are denoted by thick solid lines, while quartets of complex eigenvalues are denoted by thick dash-dotted lines.

Figure 1 corresponds to the simple cube configuration with $S_1 = \{0, \frac{\pi}{2}, \pi, \frac{3\pi}{2}\}$. As is indicated in Table 1, this configuration should be unstable due to an eigenvalue $\lambda \approx 2\epsilon^{1/2}$, of multiplicity four. What we find however is that the pair of multiple real eigenvalue splits in two identical pairs of real eigenvalues and a quartet of complex eigenvalues. To make things even more interesting, all four eigenvalues in the right-half-plane have the same real part denoted by the very thick solid line in the left panel of Fig. 1. The imaginary part of the quartet of complex eigenvalues is denoted by dash-dotted line in the right panel of the figure. If the real part of all four eigenvalues is at the order $\mathrm{O}(\epsilon^{1/2})$, the imaginary part of complex eigenvalues occurs at the order $\mathrm{O}(\epsilon)$ with a numerical approximation $\lambda \approx 2\epsilon^{1/2} \pm 2i\epsilon$. Besides these four eigenvalues in the right-half-plane, Table 1 also reports existence of a pair of double imaginary eigenvalues at the order $\mathrm{O}(\epsilon)$ and a pair of simple imaginary eigenvalues at the order $\mathrm{O}(\epsilon^3)$. All these eigenvalues are shown on the right panel of Fig. 1 by thin lines, since the pair of double imaginary eigenvalues splits into two pairs of simple imaginary eigenvalues. We can see that, although the results of Table 1 give only the leading-order approximations of small eigenvalues of the linearized problem, they represent adequately the pattern of unstable and neutrally stable eigenvalues.

Figure 2 describes another simple cube vortex configuration of Table 1 with $S_1 = \{0, \frac{3\pi}{2}, \pi, \frac{\pi}{2}\}$. As theoretically predicted, we find this configuration to be immediately unstable, due to a double pair of real eigenvalues at the order $\mathrm{O}(\epsilon^{1/2})$ and another double pair of real eigenvalues of the order $\mathrm{O}(\epsilon)$. Both

pairs split for small values of ϵ but remain simple pairs of real eigenvalues for sufficiently small values of ϵ. Then, a pair of the former and one of the latter collide for $\epsilon \approx 0.175$, leading to a quartet of complex eigenvalues. Another double pair of imaginary eigenvalues exists at the order $O(\epsilon^{1/2})$ and it splits into simple pairs of imaginary eigenvalues. When these eigenvalues meet the continuous spectrum located at $\pm i[1, 1 + 6\epsilon]$, the pairs of imaginary eigenvalues generate additional quartets of complex eigenvalues for $\epsilon > 0.113$ and $\epsilon > 0.125$. Finally, one more pair of imaginary eigenvalues exists at the order $O(\epsilon^3)$ and it remains small for $0 < \epsilon < 0.2$.

Figure 3 describes the third simple cube vortex configuration of Table 1 with $S_1 = \{\pi, \frac{3\pi}{2}, 0, \frac{\pi}{2}\}$, which is *linearly stable* for small ϵ. The quadruple pair of imaginary eigenvalues at the order $O(\epsilon^{1/2})$ splits for small ϵ into a double pair and two simple pairs of imaginary eigenvalues. All these pairs generate quartets of complex eigenvalues upon collision with the continuous spectrum for $\epsilon > 0.1$, $\epsilon > 0.125$ and $\epsilon > 0.174$. Therefore, the vortex configuration becomes unstable for sufficiently large ϵ. A double pair of imaginary eigenvalues at the order $O(\epsilon)$ splits for small ϵ into simple pairs of imaginary eigenvalues. The additional pair of imaginary eigenvalues at the order $O(\epsilon^3)$ remains small for $0 < \epsilon < 0.2$.

The double cross vortex configuration of Table 2 with $S_1 = \{0, \frac{\pi}{2}, \pi, \frac{3\pi}{2}\}$ is shown in Figure 4. It is quite interesting that both double pairs of real and imaginary eigenvalues at the order $O(\epsilon)$ split for small ϵ into simple pairs of real and imaginary eigenvalues, while the double pair of real eigenvalues at the order $O(\epsilon^2)$ remain double for small ϵ.

The double cross vortex configuration of Table 2 with $S_1 = \{0, \frac{3\pi}{2}, \pi, \frac{\pi}{2}\}$ is shown in Fig. 5. All pairs of real and imaginary eigenvalues are simple including the triple pair of imaginary eigenvalues at the order $O(\epsilon)$ which splits for small ϵ into three simple pairs of imaginary eigenvalues.

Finally, the double cross vortex configuration of Table 2 with $S_1 = \{\pi, \frac{3\pi}{2}, 0, \frac{\pi}{2}\}$ is found to be linearly stable for $\epsilon < 0.2$ and is shown in Fig. 6. The double and quadruple pairs of imaginary eigenvalues at the order $O(\epsilon)$ split for small ϵ into individual simple pairs of imaginary eigenvalues. We note that the domain of stability of this vortex cross configuration is wider than the one for the simple cube vortex configuration on Fig. 3.

Lastly, we turn to the diamond configurations of Table 3. For the case of $S_{-1} = 0$ and $S_1 = 0$, shown in Fig. 7, the configuration is unstable due to a simple and a double pair of real eigenvalues, both of $O(\epsilon)$, captured very accurately by our theoretical approximation. In addition, a complex quartet emerges because of the collision of a pair of imaginary eigenvalues with the continuous spectrum for $\epsilon > 0.175$.

The second diamond configuration with $S_{-1} = 0$ and $S_1 = \pi$, shown in Fig. 8, is unstable due to two simple pairs of real eigenvalues, one at the order $O(\epsilon)$ and one at the order $O(\epsilon^2)$. The simple pair of imaginary eigenvalues becomes a quartet of complex eigenvalues upon collision with the continuous spectrum for $\epsilon > 0.179$. The double pair of imaginary eigenvalues remains double for $0 < \epsilon < 0.2$.

Finally, the third diamond vortex configuration with $S_{-1} = \frac{\pi}{2}$ and $S_1 = \frac{3\pi}{2}$, shown in Fig. 9, is linearly stable for $0 < \epsilon < 0.2$. In this case also, the theoretical prediction accurately captures the simple pair of imaginary eigenvalues at the order $O(\epsilon)$, the triple pair of imaginary eigenvalues (splitting into a double pair and a simple one) at the order $O(\epsilon)$, and the simple pair of imaginary eigenvalues at the order $O(\epsilon^2)$.

6 Conclusion

The main benefit of the present paper is that it provides a systematic computational approach, based on a symbolic mathematical package to unravel the existence and linear stability of any configuration of interest in a three-dimensional lattice that is of paramount interest in a wide range of applications. The package implements the conditions of the Lyapunov-Schmidt reduction method that are necessary and, in the case of convergence, sufficient for persistence of relevant configurations. The reductions start from the anti-continuum limit of the lattice and extend the solution with respect to the coupling parameter ϵ. The algorithm subsequently connects the leading-order behavior of the small eigenvalues of the stability problem (which bifurcate from the zero eigenvalue at $\epsilon = 0$ and are responsible for the instability of the vortex configurations) to the Jacobian matrix of the above conditions. In so doing, it provides a powerful predictor that we have always found to be accurate for small values of the coupling parameter (typically for $\epsilon < 0.1$). We thus believe that this work provides a valuable tool that can be used to examine various configurations that may be of interest to both theoretical and experimental studies in optical and soft-condensed-matter systems.

Acknowledgement. M. L. is supported by the NSERC USRA scholarship. D.P. is supported by the NSERC Discovery grant and the EPSRC Research Fellowship. P.G.K. is supported by NSF through the grants DMS-0204585, DMS-CAREER, DMS-0505663 and DMS-0619492.

A Outputs of the computational algorithm

A.1 Output of Algorithm 1

Jacobian matrix at the 1st order:

$$M1 = \begin{bmatrix} -1 & 0 & 0 & 0 & 1 & 0 & 0 & 0 \\ 0 & -1 & 0 & 0 & 0 & 1 & 0 & 0 \\ 0 & 0 & -1 & 0 & 0 & 0 & 1 & 0 \\ 0 & 0 & 0 & -1 & 0 & 0 & 0 & 1 \\ 1 & 0 & 0 & 0 & -1 & 0 & 0 & 0 \\ 0 & 1 & 0 & 0 & 0 & -1 & 0 & 0 \\ 0 & 0 & 1 & 0 & 0 & 0 & -1 & 0 \\ 0 & 0 & 0 & 1 & 0 & 0 & 0 & -1 \end{bmatrix}$$

Non-zero eigenvalues of $M1$:

$$u[1] = -2, \quad u[2] = -2, \quad u[3] = -2, \quad u[4] = -2$$

Projection of $M2$ to Null($M1$):

$$M2 = \begin{bmatrix} 1 & 0 & 0 & -1 \\ 0 & 1 & -1 & 0 \\ 0 & -1 & 1 & 0 \\ -1 & 0 & 0 & 1 \end{bmatrix}$$

Non-zero eigenvalues of $M2$:

$$u[5] = 2, \quad u[6] = 2$$

Projection of $M3$ to Null($M2$):

$$M3 = \begin{bmatrix} 0 & 0 \\ 0 & 0 \end{bmatrix}$$

Projection of $M4$ to Null($M2$):

$$M4 = \begin{bmatrix} 0 & 0 \\ 0 & 0 \end{bmatrix}$$

Projection of $M5$ to Null($M2$):

$$M5 = \begin{bmatrix} 0 & 0 \\ 0 & 0 \end{bmatrix}$$

Projection of $M6$ to Null($M2$):

$$M6 = \begin{bmatrix} -8 & 8 \\ 8 & -8 \end{bmatrix}$$

Non-zero eigenvalues of $M6$:

$$u[7] = -16$$

A.2 Output of Algorithm 2

Projection of $i\sigma H - \lambda I$ at 1st order:

$$\begin{bmatrix} -1-\frac{1}{2}\lambda^2 & 0 & 0 & 0 & 1 & 0 & 0 & 0 \\ 0 & -1-\frac{1}{2}\lambda^2 & 0 & 0 & 0 & 1 & 0 & 0 \\ 0 & 0 & -1-\frac{1}{2}\lambda^2 & 0 & 0 & 0 & 1 & 0 \\ 0 & 0 & 0 & -1-\frac{1}{2}\lambda^2 & 0 & 0 & 0 & 1 \\ 1 & 0 & 0 & 0 & -1-\frac{1}{2}\lambda^2 & 0 & 0 & 0 \\ 0 & 1 & 0 & 0 & 0 & -1-\frac{1}{2}\lambda^2 & 0 & 0 \\ 0 & 0 & 1 & 0 & 0 & 0 & -1-\frac{1}{2}\lambda^2 & 0 \\ 0 & 0 & 0 & 1 & 0 & 0 & 0 & -1-\frac{1}{2}\lambda^2 \end{bmatrix}$$

Non-zero eigenvalues of $i\sigma H - \lambda I$ at 1st order:

$$w[1] = -2i, \;\; w[2] = -2i, \;\; w[3] = -2i, \;\; w[4] = -2i, \;\; w[5] = 2i, \;\; w[6] = 2i, \;\; w[7] = 2i, \;\; w[8] = 2i$$

Projection of $i\sigma H - \lambda I$ at 2nd order:

$$\begin{bmatrix} 1-\frac{1}{2}\lambda^2 & -\lambda & \lambda & -1 \\ \lambda & 1-\frac{1}{2}\lambda^2 & -1 & -\lambda \\ -\lambda & -1 & 1-\frac{1}{2}\lambda^2 & \lambda \\ -1 & \lambda & -\lambda & 1-\frac{1}{2}\lambda^2 \end{bmatrix}$$

Non-zero eigenvalues of $i\sigma H - \lambda I$ at 2nd order:

$$w[9] = -2i, \;\; w[10] = -2i, \;\; w[11] = 2i, \;\; w[12] = 2i$$

Projection of $i\sigma H - \lambda I$ at 3rd order:

$$M3 = \begin{bmatrix} -\frac{1}{2}\lambda^2 & 0 \\ 0 & -\frac{1}{2}\lambda^2 \end{bmatrix}$$

Projection of $i\sigma H - \lambda I$ at 4th order:

$$M4 = \begin{bmatrix} -\frac{1}{2}\lambda^2 & 0 \\ 0 & -\frac{1}{2}\lambda^2 \end{bmatrix}$$

Projection of $i\sigma H - \lambda I$ at 5th order:

$$M5 = \begin{bmatrix} -\frac{1}{2}\lambda^2 & 0 \\ 0 & -\frac{1}{2}\lambda^2 \end{bmatrix}$$

Projection of $i\sigma H - \lambda I$ at 6th order:

$$M6 = \begin{bmatrix} -8 - \frac{1}{2}\lambda^2 & 8 \\ 8 & -8 - \frac{1}{2}\lambda^2 \end{bmatrix}$$

Non-zero eigenvalues of $i\sigma H - \lambda I$ at 6th order:

$$w[13] = -4i \text{ Sqrt}[2], \quad w[14] = 4i \text{ Sqrt}[2]$$

References

[1] D. N. Christodoulides, F. Lederer and Y. Silberberg, Nature **424**, 817-823 (2003).

[2] J.W. Fleischer, G. Bartal, O. Cohen, T. Schwartz, O. Manela, B. Freeman, M. Segev, H. Buljan, and N.K. Efremidis, Optics Express **13**, 1780-1796 (2005).

[3] V.V. Konotop and V.A. Brazhnyi, Mod. Phys. Lett. B **18** 627-651, (2004); O. Morsch and M. Oberthaler, Rev. Mod. Phys. **78**, 179-215 (2006); P.G. Kevrekidis and D.J. Frantzeskakis, Mod. Phys. Lett. B **18**, 173-202 (2004).

[4] P. Binder, D. Abraimov, A. V. Ustinov, S. Flach, and Y. Zolotaryuk, Phys. Rev. Lett. **84**, 745-748 (2000); E. Trías, J.J. Mazo, and T.P. Orlando, Phys. Rev. Lett. **84**, 741-744 (2000).

[5] M. Sato, B. E. Hubbard, and A. J. Sievers, Rev. Mod. Phys. **78**, 137-157 (2006).

[6] M. Peyrard, Nonlinearity **17**, R1-R40 (2004).

[7] S. Aubry, Physica D **103**, 201-250, (1997); S. Flach and C.R. Willis, Phys. Rep. **295** 181-264 (1998); D. Hennig and G. Tsironis, Phys. Rep. **307**, 333-432 (1999).

[8] P.G. Kevrekidis, K.Ø. Rasmussen and A.R. Bishop, Int. J. Mod. Phys. B **15**, 2833-2900 (2001); J.C. Eilbeck and M. Johansson, in *Proceedings of the 3rd Conference on Localization and Energy Transfer in Nonlinear Systems*, Eds. L. Vazquez et al. (World Scientific, New Jersey, 2003), pp. 44-67.

[9] C. Sulem and P.L. Sulem, *The Nonlinear Schrödinger Equation*, Springer-Verlag (New York, 1999).

[10] D.N. Christodoulides and R.I. Joseph, Opt. Lett. **13**, 794-796 (1988).

[11] G.L. Alfimov, P.G. Kevrekidis, V.V. Konotop and M. Salerno, Phys. Rev. E **66**, 046608 (2002); N.K. Efremidis and D.N. Christodoulides, Phys. Rev. A **67**, 063608 (2003).

[12] H. S. Eisenberg, Y. Silberberg, R. Morandotti, A. R. Boyd, and J. S. Aitchison, Phys. Rev. Lett. **81**, 3383-3386 (1998).

[13] R. Morandotti, U. Peschel, J. S. Aitchison, H. S. Eisenberg, and Y. Silberberg , Phys. Rev. Lett. **83**, 2726-2729 (1999).

[14] J. Meier, G. I. Stegeman, D. N. Christodoulides, Y. Silberberg, R. Morandotti, H. Yang, G. Salamo, M. Sorel, and J. S. Aitchison, Phys. Rev. Lett. **92**, 163902 (2004).

[15] A. Smerzi, A. Trombettoni, P.G. Kevrekidis and A.R. Bishop, Phys. Rev. Lett. **89**, 170402 (2002); F.S. Cataliotti, L. Fallani, F. Ferlaino, C. Fort, P. Maddaloni and M. Inguscio, New J. Phys. **5**, 71 (2003).

[16] D.N. Neshev, T.J. Alexander, E.A. Ostrovskaya, Yu.S. Kivshar, H. Martin, I. Makasyuk, and Z. Chen, Phys. Rev. Lett. **92**, 123903 (2004); J.W. Fleischer, G. Bartal, O. Cohen, O. Manela, M. Segev, J. Hudock, and D.N. Christodoulides, Phys. Rev. Lett. **92**, 123904 (2004).

[17] D.E. Pelinovsky, P.G. Kevrekidis and D.J. Frantzeskakis, Physica D **212**, 1-19 (2005).

[18] D.E. Pelinovsky, P.G. Kevrekidis, and D. Frantzeskakis, Physica D **212**, 20-53 (2005)

[19] P.G. Kevrekidis and D.E. Pelinovsky, Proceedings of the Royal Society A **462**, 2671-2694 (2006).

[20] P.G. Kevrekidis, B. A. Malomed, D. J. Frantzeskakis and R. Carretero-González, Phys. Rev. Lett. **93**, 080403 (2004).

[21] R. Carretero-González, P.G. Kevrekidis, B.A. Malomed, and D.J. Frantzeskakis, Phys. Rev. Lett. **94**, 203901 (2005).

[22] J.E. Heebner and R.W. Boyd, J. Mod. Opt. **49**, 2629-2636 (2002); P. Chak, J.E. Sipe, and S. Pereira, Opt. Lett. **28**, 1966-1968 (2003).

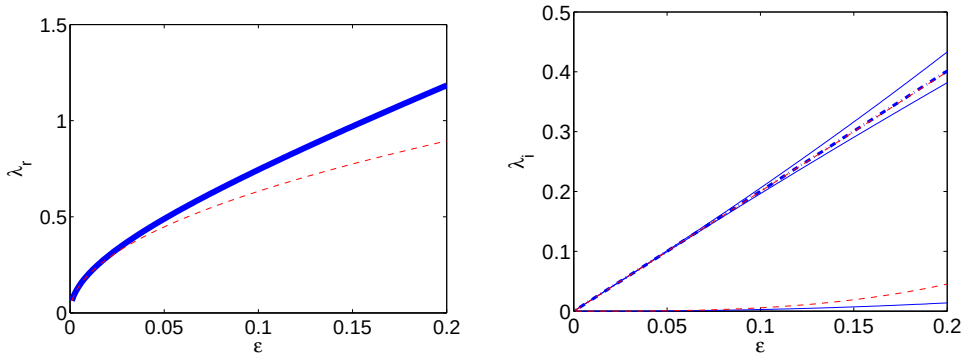

Figure 1: The real (left) and imaginary (right) parts of small eigenvalues of the linearized problem (2.6) associated with the simple cube vortex configuration with $S_1 = \{0, \frac{\pi}{2}, \pi, \frac{3\pi}{2}\}$ versus ϵ; see the first paragraph of Section 5 for the meaning of the different lines.

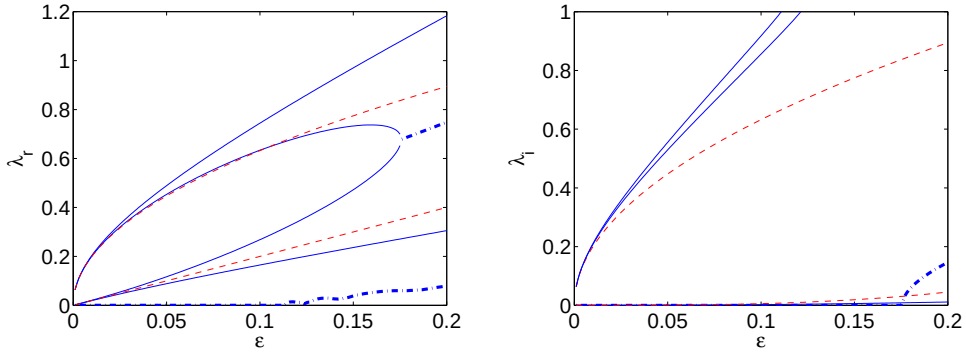

Figure 2: Same as in Fig. 1, but for the simple cube vortex configuration with $S_1 = \{0, \frac{3\pi}{2}, \pi, \frac{\pi}{2}\}$.

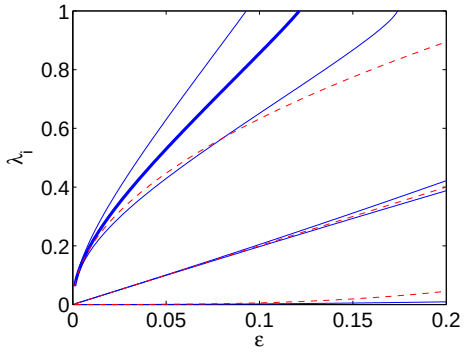

Figure 3: Same as in Fig. 1, but for the stable simple cube vortex configuration with $S_1 = \{\pi, \frac{3\pi}{2}, 0, \frac{\pi}{2}\}$.

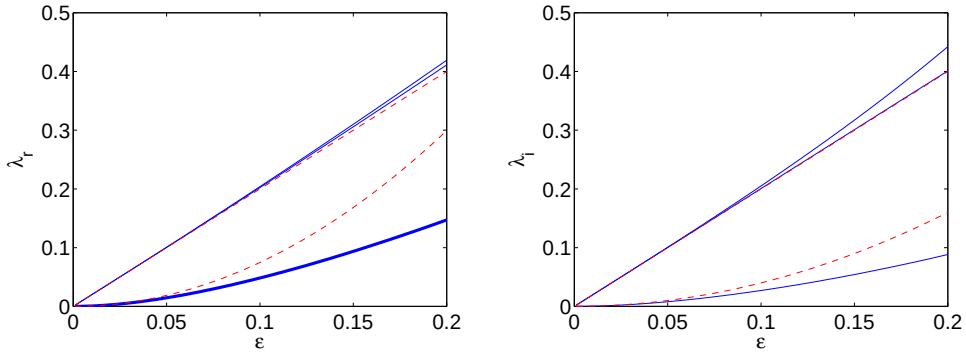

Figure 4: Same as Fig. 1, but for the double cross vortex configuration with $S_1 = \{0, \frac{\pi}{2}, \pi, \frac{3\pi}{2}\}$.

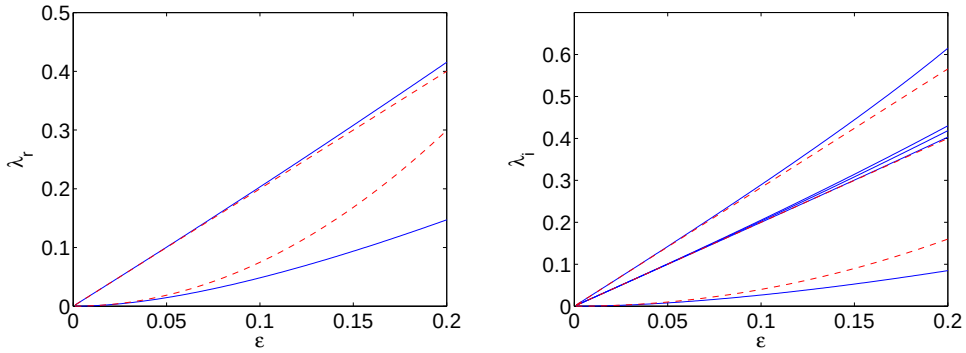

Figure 5: Same as Fig. 1, but for the double cross vortex configuration with $S_1 = \{0, \frac{3\pi}{2}, \pi, \frac{\pi}{2}\}$.

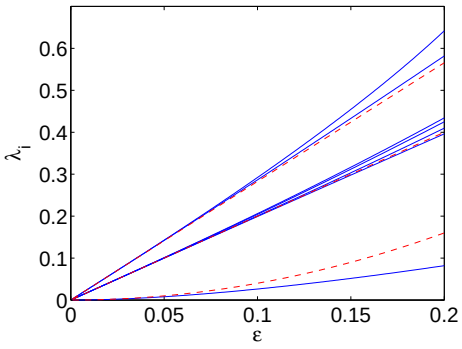

Figure 6: Same as Fig. 1, but for the stable double cross vortex configuration with $S_1 = \{\pi, \frac{3\pi}{2}, 0, \frac{\pi}{2}\}$.

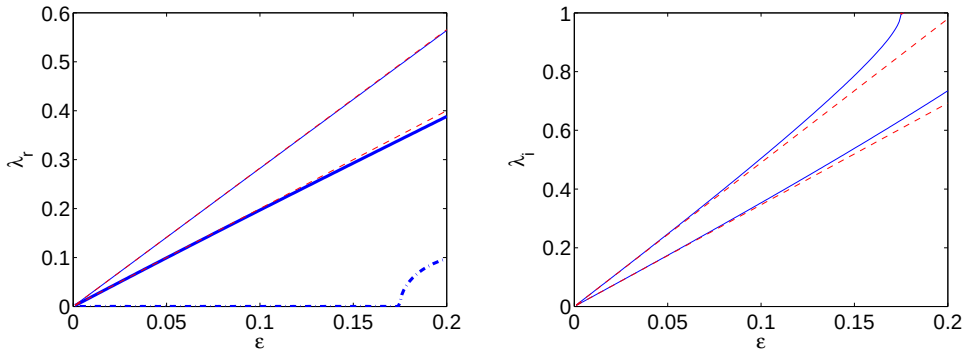

Figure 7: The real and imaginary parts of the pertinent eigenvalues of the diamond configuration with $S_{-1} = 0$ and $S_1 = 0$ as a function of ϵ.

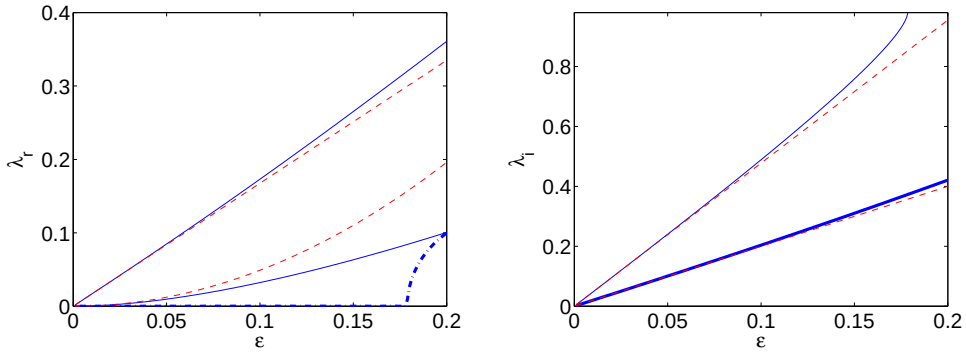

Figure 8: Same as in Fig. 7, but for the diamond configuration with $S_{-1} = 0$ and $S_1 = \pi$.

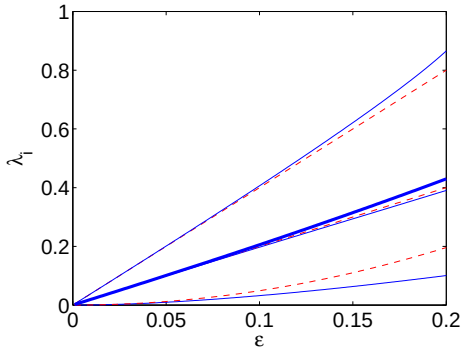

Figure 9: Same as in Fig. 7, but for the stable diamond vortex configuration with $S_{-1} = \frac{\pi}{2}$ and $S_1 = \frac{3\pi}{2}$.